Trailing Vortices around a 45° Pitched-Blade Impeller

M. Schäfer, M. Yianneskis, P. Wächter, and F. Durst
Lehrstuhl für Strömungsmechanik, Universität Erlangen-Nürnberg, Cauerstraβe 4, 91058 Erlangen, Germany

The trailing vortex system near impeller blades has been identified as the major flow mechanism responsible for mixing and dispersion in stirred vessels, and high turbulence levels in the vortices have an important impact on such phenomena as drop breakup and cell damage in bioreactors. Numerical computations of the flows require more detailed information on the velocity characteristics generated by different impeller designs than is available in the literature. Our study on the mean flow and turbulence structure generated by a pitched-blade turbine with four 45° inclined blades found that single trailing vortex is formed around each turbine blade. The vortex axis spread out radially by less than 0.0015 T and was inclined at 20° to the horizontal plane. The vortices merged into the bulk flow structure at around 135° behind each blade. Periodicity of the mean flow due to the crossing of the individual blades and high levels of kinetic energy of turbulence (k) are contained within a radial distance of around $r/T = 0.23$ from the axis and a vertical distance of $z/T = 0.07 - 0.46$ from the bottom of the vessel. The k levels decay to nearly-uniform and low values outside this region. The results are compared with earlier investigations, and their implications for mixing processes and CFD predictions of the flows are discussed. The data identify flow regions accurately where intense turbulence is present and thus give useful indications for the optimization of mixing processes.

Introduction and Brief Literature Survey

The complex nature of the flow fields in stirred chemical reactors has motivated a number of studies of the mean velocity and turbulence characteristics of the flows produced by different impeller designs. Numerous publications are available that document power number–Reynolds number ($N_p - Re$) relationships for various impeller configurations. Some publications also report velocity information. Most of these investigations have been concerned with the flow in vessels stirred by a single Rushton impeller (see, for example, van't Riet et al., 1976; Yianneskis et al., 1987; Wu and Patterson, 1989; Stoots and Calabrese, 1995; Höfken et al., 1996; and Schäfer et al., 1997). These investigations have identified the formation of a trailing vortex pair behind each impeller blade and reported that the 360° ensemble-averaged turbulence levels measured in the impeller stream may be overestimated by the associated variation in mean velocity. Even though the flow in the impeller vicinity of stirred-reactor vessels is periodic, ensemble-averaged LDA measurements obtained over 360° of impeller revolution are widely employed for the description of the velocity and turbulence fields. These measurements do not account for the broadening of the rms levels caused by the mean flow variation due to the blade passage (van't Riet et al., 1976). Angle-resolved LDA measurements over where the data were arranged in 1° averages do show the variation of the mean flow velocities and the turbulence fluctuations with blade angle ϕ, and it has been shown that in comparison with 1° angle-resolved measurements, 360° ensemble-averaged measurements can lead to an overestimation of turbulence quantities in the impeller stream by up to 400% (Yianneskis and Whitelaw, 1993).

Pitched-blade turbines (PBTs) are commonly used in industrial mixing applications, partly because they are more ef-

Correspondence concerning this article should be addressed to M. Yianneskis at Dept. of Mechanical Engineering, King's College London, Strand, London WC2R 2LS, U.K..

ficient than Rushton turbines, for example, for processes requiring solid suspension (see, for example, Zwietering, 1958; and Rao et al., 1988, but they are also used in gas dispersion systems. The trailing vortices formed behind the blades have a low-pressure core. These low-pressure regions do not contribute to the drag portion of the power consumption of the impeller (Tay and Tatterson, 1985), but may coalesce sparged gas to form gas cavities behind the blades. The trailing vortices have been identified as very important for ligament and sheet production in liquid–liquid dispersion, as shown by Ali et al. (1981) and Sheu et al (1982), who emphasized that the trailing vortex system is the major flow mechanism responsible for dispersion. In addition, the information available on stirred-vessel flows driven by pitched-blade impellers is incomplete as far as the data needed for CFD developments are concerned. More detailed and precise angle-resolved measurements are needed to yield the mean velocity and turbulence information required for comparison with corresponding predictions. The preceding observations have motivated the work presented in this article.

Nouri and Whitelaw (1990a) have reported a change in mean flow pattern produced by PBTs with Reynolds number. Hockey (1990) also reported a similar change in the discharge stream direction from primarily radial to primarily axial flow with 45° and 60° PBTs, which in his 144-mm-diameter vessel occurred at *Re*'s of 490 and 650, respectively. Hockey and Nouri (1996) reported a sudden drop in the power number measured with a $D = T/3$ 60° six-bladed PBT in a 294-mm vessel at $Re = 1{,}200$, which was associated with the transition of the flow pattern from radial to axial flow that was observed visually. Distelhoff et al.'s (1995) power measurements in a 144-mm tank with a similar 60° PBT also showed a similar transition at $Re = 650$. Tatterson and Stanford (1981) reported that the flow produced by a 45° four-bladed PBT in their 914-mm-dia. vessel was entirely laminar at an impeller Reynolds number of 1300. The results just outlined show clearly the dependency of the flow patterns produced by PBTs on the Reynolds number.

Armstrong and Ruszkowski (1987) reported the mean axial and tangential velocities in the stream emerging from a 45° PBT; they found that the tangential velocity is proportional to the radius, and that the axial mean velocity reached a maximum of 0.5 V_{tip}. Ranade and Joshi (1989) studied the flows produced with a range of PBTs and found that the turbine hydraulic efficiency increases with blade pitch; they carried out ensemble-averaged LDA measurements with a six-blade 45° PBT of diameter $D = T/3$ located at a clearance of $C = T/3$, and reported that the mean and rms velocities scaled with *Re* in the range $40{,}000 < Re < 140{,}000$. The results presented indicated that the flow is directed upward over the outer part of the impeller, but, as Kresta and Wood (1993a) point out, this was due to an error in Ranade and Joshi's labeling of coordinates in the article. The bulk-flow patterns with 45° PBTs were reported to be different for low and high off-bottom clearances by Jaworski et al. (1991) for six-blade and Kresta and Wood (1993a) for four-blade turbines. Hockey and Nouri (1996) employed a six-blade 60° PBT and measured mean and rms velocities in the bulk flow and around the turbine using ensemble-averaged and angle-resolved LDA techniques, respectively, and reported a peak velocity of 0.55 V_{tip}.

Ali et al. (1981) observed that only a single trailing vortex was formed at the trailing edge of a four-blade 45° PBT, while Kresta and Wood (1993a) reported that a trailing vortex extending over approximately 20% of the blade was formed at the lower tip of the blade and a smaller one at the top corner of the blade. Tay and Tatterson (1985) reported that the flow over a PBT blade contains boundary layers on the front and back of the blade, a wake behind the blade, and a trailing vortex on the blade tip. However, they indicated that the wake region behind the blade was not significant and the flow resembles a boundary layer. Tatterson et al. (1980) studied the trailing vortices produced by two turbines with 45° blades, a 6-blade PBT in a 295-mm-diameter vessel, and a four blade PBT in a 914-mm vessel. Differences in the flow structures produced by the two impellers were found, but it could not be established which were due to the vessel scale and which due to the number of blades. In general, the vortical structures generated by the six-blade PBT were not as well defined. The four-blade geometry is similar to the present one, and the relevant findings are outlined below: the trailing vortex travels with the same velocity as the blade and moves slightly radially outward with a small downward vertical velocity. By the time the next blade passes, the shed vortex is found below the blade. The velocity difference between the front and back of the blade generates the circulation necessary to drive the trailing vortex. For the $D = T/3$ geometry studied, at $Re = 385{,}000$ the vortices could not be distinguished at a distance of $C/3$ of the way to the vessel bottom.

Sheu et al. (1982) developed a stereoscopic 3-dimensional (3-D) measurement technique with which they examined the flows around both Rushton and pitched-blade turbines. They found that the vortices produced by the PBTs had a spiral or helical axis. Ali et al. (1981) observed that the vortex circumferential velocities for the PBT were around 0.25 V_{tip} for all rotational speeds studied. Ali et al. observed that the diameter of the vortex was smallest behind the trailing edge of the blade and expanded linearly with distance from the trailing edge of the blade as more fluid entrained into the vortex. The vortex diameter was estimated as 0.25–0.33 of the distance from the blade tip for all speeds studied, and the shape and size of the vortices remained fairly consistent for all the observations. The convected angle of the vortex, that is, the angle between the arc formed by the horizontal plane defined by the sweep of the top tip of the blade and the edge of the trailing vortex structure, was around 18°, 15°, and 13° at 73, 115 and 153 rev/min. respectively.

Most of the investigations reported to date have been concerned with 60° PBTs and/or with the mean and rms velocities in the bulk of the vessel or at least outside the impeller swept volume. The only investigations concerned primarily with the trailing vortex structure were the flow visualization studies of Tatterson and coworkers, but the understanding and quantification of the vortex mean flow and turbulence structure is still far from complete. The main aims of the present study are to characterize the trailing vortex structure in the discharge stream and between the blades of a pitched-blade turbine, and to provide detailed angle-resolved LDA data that may be used for the assessment of CFD predictions of the flows. As stated earlier, the vortices are considered an important mechanism for dispersion, as well as for drop breakup in liquid–liquid mixing, and it is generally expected

that most of the mixing in stirred reactors takes place in the region dominated by these vortices. In addition, the high levels of turbulence in the vortices may have an important impact on phenomena such as cell damage in bioreactors. The flow in the remainder of the vessel is also considered for completeness. The results are compared with previously reported measurements where appropriate.

Flow Configuration and Experimental Techniques

Stirred-vessel configuration

The experiments were made in a cylindrical vessel of diameter $T = 152$ mm, and the liquid height in the vessel was $H = T$. Figures 1a and 1b show the geometry of the mixing vessel. Four equally spaced vertical baffles of width $B = T/10$ and thickness of 3 mm were fitted along the periphery of the vessel with a gap of 2.6 mm between the vessel wall and the end of each baffle. The vessel was made of clear cast Duran glass and was located inside a transparent glass trough. The baffles and impeller blades were also made from Duran glass. The vessel could be rotated about its axis to enable measurements to be performed at different vertical planes. The gap between the vessel and the trough was filled with the working fluid, and its temperature was controlled with a cooling coil that removed the heat generated by the impeller, and thus maintained both the temperature inside the vessel, as well as the refractive index of the fluid in the vessel and trough constant during the experiments.

The turbine was a four-bladed impeller of diameter $D = 0.329\ T$, that is, 50 mm. The blade thickness was 0.9 mm and all blade edges were square, that is, not rounded. The blade height, W, was $0.264D$ (13.2 mm), and the blade pitch was 45°. The clearance between the bottom of the mixing vessel and the middle of the impeller blades was $C = T/3$. The working fluid was silicon oil of density 1,039 kg/m^3 and dynamic viscosity 0.0159 Pa·s. Most measurements were conducted at a Reynolds number ($Re = ND^2/\nu$) of 7,300, which corresponded to an impeller rotational speed of $N = 2{,}672$ rev/min ($V_{tip} = 7$ m/s). The impeller rotated in a clockwise direction as viewed from above. LDA measurements were also made at two other Re's to establish that the results at different rotational speeds were similar, as described later. The origin of the coordinate system used is the center of the base of the vessel. To allow comparisons with measurements made in vessels of different sizes, all distances are normalized with the vessel diameter T, and all locations are described in terms of normalized axial (z/T), normalized radial (r/T), and tangential (angle θ with respect to the vessel wall) coordinates. Measurements of all three velocity components were performed in the $\theta = 0°$ plane, located half-way between two baffles. The angular location of the measurement volume with respect to the leading blade for the angle-resolved measurements is expressed as the blade angle ϕ: $\phi = 0°$ is the vertical plane through the middle of the leading blade. An optical shaft encoder that provided a marker pulse and a train of 1,000 pulses per revolution was coupled to the impeller shaft. The pulses were input to the counter and the rotational speed of the impeller could be measured. The midpoint of a blade of the impeller was aligned with the marker pulse, and by counting the number of pulses relative to the marker pulse, the blade angle ϕ could be determined.

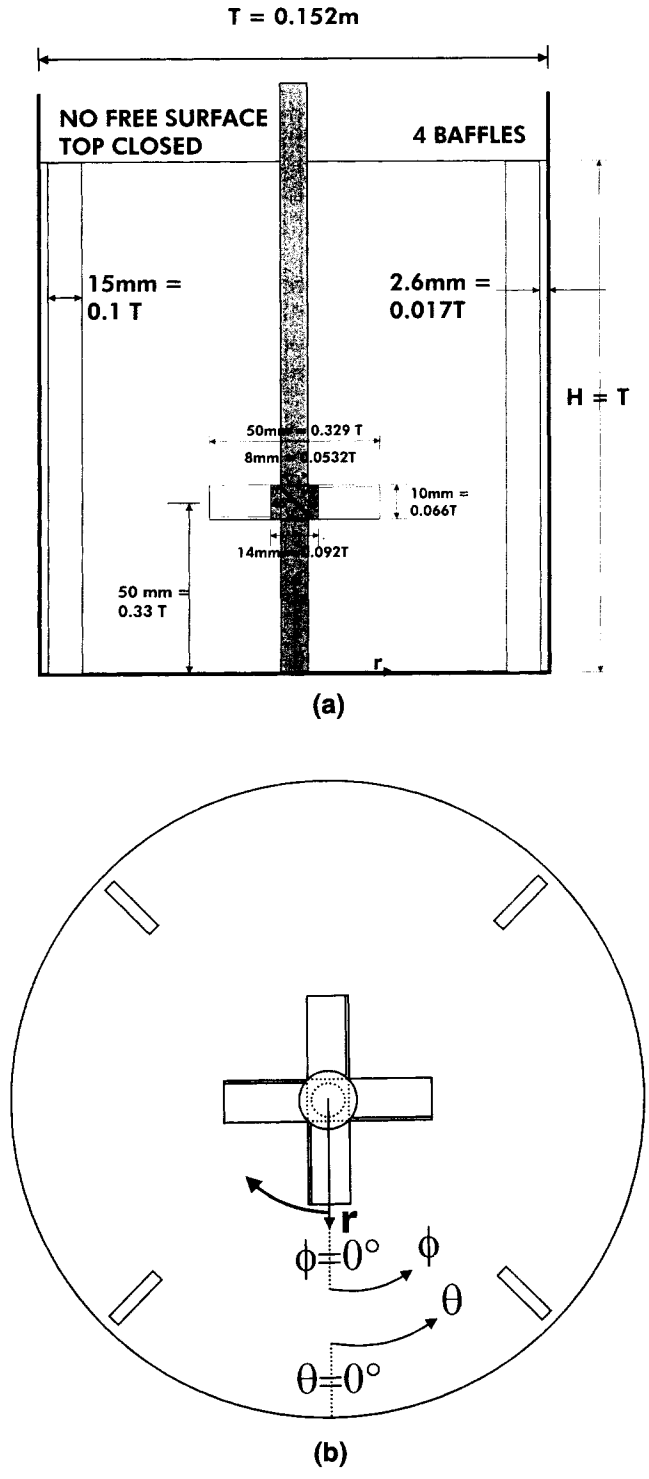

Figure 1. Stirred vessel configuration and coordinate system: (a) cross-sectional view; (b) plan view.

A lid was located above the liquid surface at a height $H = T$ so that no air bubbles were entrained into the liquid from the free surface. The effect of a lid on the flow in a stirred vessel was previously investigated by Nouri and Whitelaw (1990b), who concluded that the use of a lid only affects the flow in the immediate vicinity of the lid–free surface and that the

velocities elsewhere in a 144-mm vessel were almost identical to those in a 294-mm vessel.

Angle-resolved measurements were made of the axial, radial, and tangential mean velocity components ($\overline{U}, \overline{V}$, and $\overline{W}$, respectively); and of the corresponding turbulence levels (u', v', and w', respectively), at 582 locations in the vicinity of the impeller stream with a measurement location spacing of 1–2 mm and 629 locations in the bulk of the vessel with a spacing of 4 mm. The finer measurement grid around the impeller was selected in order to reveal in detail the structure of the trailing vortices. In order to resolve the flow motion relative to the rotating blade, the rotational velocity V_r was subtracted from the angle-resolved mean tangential velocities. V_r was defined as

$$V_r = \frac{2\pi Nr}{60} \text{ (m/s)}, \tag{1}$$

where N is the impeller rotational speed in revolutions per minute and r is the radial distance from the axis of the vessel to the point of measurement.

For the purpose of comparison with data obtained in vessels of different sizes, all angle-resolved mean velocities have been normalized with the blade-tip velocity $V_{tip} = \pi ND/60$ and are denoted by $\overline{U}/V_{tip}$, $\overline{V}/V_{tip}$, and $\overline{W}/V_{tip}$, respectively, for the axial, radial, and tangential components. The turbulence level results were also normalized with V_{tip} and are denoted by u'/V_{tip}, v'/V_{tip} and w'/V_{tip} for the axial, radial, and tangential components, respectively. Angle-resolved turbulence kinetic energy results were obtained from the u', v', and w' data using:

$$k = \frac{1}{2}(u'^2 + v'^2 + w'^2). \tag{2}$$

The turbulence kinetic energy results were normalized with V_{tip}^2 and the corresponding values are denoted by k/V_{tip}^2.

To facilitate interpretation of the results, the outline of the blades, hub, and shaft is drawn to scale in all figures depicting the results. In the figures depicting results in horizontal (z) planes, the impeller should be considered to be rotating clockwise, while in those depicting results in vertical (ϕ or θ) planes, the impeller should be considered to be moving out of the plane of the paper toward the viewer. In order to aid the interpretation of the results, a reference scale having the magnitude of 0.4–0.5 V_{tip} is drawn in each figure depicting angle-resolved mean velocity vectors. Turbulence kinetic energy results are plotted in contour form.

Laser-Doppler anemometer and experimental techniques

The anemometer comprised a 100-mW monomode laser diode, associated lenses, and a Bragg cell that provided a frequency shift of 2 MHz between the two beams. The laser light was transmitted with optical fibers to the optical system consisting of a beam splitter, Bragg cell, fiber coupler, a set of fiber optics, and an optical probe; the latter was mounted on a frame that could be traversed in three orthogonal directions by means of stepper motors controlled with a computer program. There was no displacement of the measurement volume due to refraction, as the refractive index of the glass cylinder, baffles, blades, and trough was matched to that of the working fluid at 21°C. The accuracy in traversing the optical bench in the three directions was 0.1 mm. The bench was aligned to the test section, and the plane of the beams could be rotated so that they could be placed in either a vertical or horizontal plane. The radial and tangential velocity components were measured with the beams located in a horizontal and the axial velocity component with the beams in a vertical plane. The working fluid was seeded with titanium dioxide particles of 3-μm mean diameter. The backscattered light produced when these particles crossed through the measurement volume was focused onto the photomultiplier.

A frequency counter (TSI model 1980B) was used for the LDA measurements. The signal from the photomultiplier was filtered to remove low-frequency pedestal and high-frequency noise and then amplified by a variable gain; the quality of the signal was continously monitored with an oscilloscope. The counter was interfaced with a PC. The interface was controlled by a computer program to acquire data from the counter as well as the arrival time/angle of the data. The width of the measurement interval was set to enable acquisition of data between a specified 90° interval (i.e., between two neighboring blades). For each measurement, 60,000 and 10,000 angle-resolved velocity data were collected over this interval in the impeller vicinity and bulk flows, respectively. The velocity data and their corresponding angles were then saved on a disk file for off-line processing. The uncertainty in aligning the marker pulse with the impeller blade was 0.36°.

There are a number of possible error sources in an LDA system, and measurement uncertainties vary with location. The variation of impeller speed was kept within ± 30 rev/min (1%). The accumulated errors in the mean and rms velocity measurements have been estimated to be, on average, 1–3% and 5–10% of V_{tip}, respectively, with the higher errors expected in regions of steep velocity gradients.

Experimental Results and Discussion

Flow visualization

The flow patterns were observed with laser-sheet flow visualization to determine qualitatively the mean flow structure in the range $225 < Re < 7{,}500$. All observations were made in the $\theta = 0°$ plane, located half-way between two baffles. At $Re = 225$ the flow stream discharged from the impeller in a primarily radial direction, with part of the flow recirculating along the vessel bottom toward the impeller. The main flow feature was a circulation loop formed by the impeller stream that flowed up the vessel wall and then turned toward the top of the impeller. A second, smaller circulation formed below the impeller hub, which as Re was increased, extended at times to the bottom of the impeller. At $Re = 490$–500 the impeller discharge flow direction was unstable, varying from radial to axial. The observed transition from radial to axial flow compares favorably with the observations of Hockey (1990), who reported a similar change at $Re = 490$ in a 144-mm vessel. At $Re = 1{,}100$ the flow was primarily in the axial direction and the main circulation loop extended in height to reach as far as $z/T = 0.5$ above the impeller. This axial flow reached the vessel bottom at around $r/T = 0.25$ for $Re > 1100$. The small secondary circulation decreased in size with in-

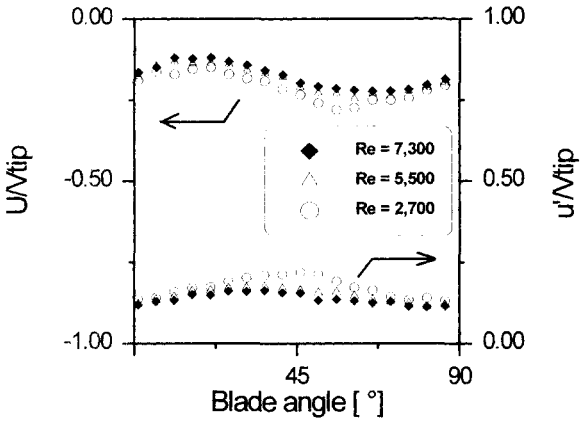

Figure 2. Variation of normalized axial mean ($\bar{U}/V_{tip}$) and rms (u'/V_{tip}) velocities with blade angle (ϕ) at $z/T = 0.23$, $r/T = 0.164$ for Reynolds numbers of 2,700, 5,500, and 7,300.

creasing Re and by $Re = 2300$ it was less than 0.1 T in diameter. For $Re > 2300$ the direction of the impeller discharge was always very stable and the main circulation loop extended to around 0.5–0.66 T from the vessel bottom.

In order to establish that the flow velocities scaled with rotational speed for Re's higher than that required for the impeller flow direction to become primarily axial, especially as it is normally expected that the lower limit for fully turbulent flow is $Re = 20{,}000$, angle-resolved measurements were made in a number of locations in the impeller stream and bulk flow. Characteristic axial mean and rms velocity profiles (normalized with V_{tip}) obtained at $z/T = 0.23$ and $r/T = 0.164$, for $Re = 2{,}700$, 5,500, and 7,300, are shown in Figure 2. It can be seen that both the normalized mean and rms profiles at the two higher Re's are identical within 0.02 V_{tip}, that is, essentially within the precision of the instrument. The flow visualization observations and LDA data just cited indicate that the flow is turbulent and the flow pattern is primarily axial for $Re > 2{,}300$.

90° Ensemble-averaged mean velocity measurements

The mean velocity vector field in the $\theta = 0°$ plane obtained from 90° ensemble-averaged measurements is shown in Figure 3. The flow features from the flow visualization experiments just described can be observed in the LDA results as well: the nearly axial direction of the discharge flow immediately below the impeller, which becomes increasingly more radial and reaches the bottom at around $r/T = 0.25$, the small vortex below the hub that is around 0.1 T in diameter, and the main circulation loop reaching $z/T = 0.55$–0.65. It can be seen from this figure that the velocities near the top third of the vessel are small, well below 0.05 V_{tip}, while the ascending flow along the cylinder wall has magnitudes of around 0.20 V_{tip}. The velocities in the vortex below the hub are very small, and this indicates that there may be problems with lifting solids off the bottom in this area in solid–liquid systems.

The peak axial mean velocity, measured immediately below the impeller near $r/T = 0.125$, is around 0.45 V_{tip}, in close agreement with the value reported by Kresta and Wood (1993a), while Armstrong and Ruszkowski (1987) reported the

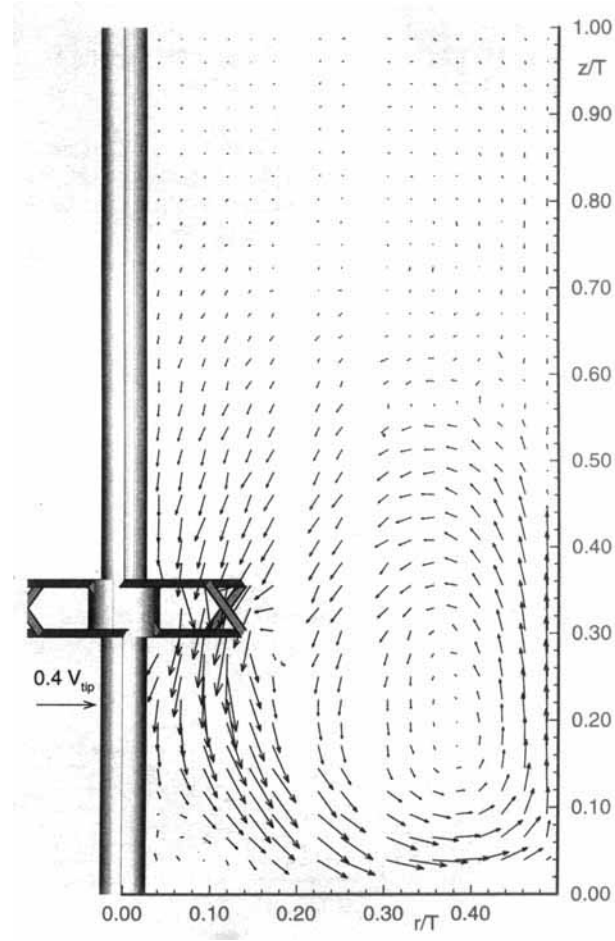

Figure 3. Ensemble-averaged mean velocity vectors in the $\theta = 0°$ plane.

slightly higher value of 0.5 V_{tip}. Kresta and Wood associated this peak with the presence of the trailing vortices; this is, broadly speaking, correct: the data presented below will show that the vortex is centered around a radius of 0.16 T in that region and that the maximum of the axial velocity is encountered at the edge of the vortex.

Angle-resolved mean velocity measurements and trailing vortex structure

The ensemble-averaged measurements presented earlier were calculated from angle-resolved LDA data averaged over 1° of impeller revolution. Extensive checks were made to establish the region around the impeller in which the periodicity due to the crossing of the blades could be detected. It was found that this periodicity was entirely contained within a cylindrical region of radius equal to 0.23 T and height 0.39 T, that is, extending from the axis of the vessel to $r/T = 0.23$ and over $0.07 < z/T < 0.46$. Outside this region the mean velocity variation with blade angle ϕ was free from periodic fluctuations due to blade crossings. Within this region where periodic flow was dominant, detailed measurements (in most areas measurement locations were only 1 mm apart) were made in order to resolve the trailing vortex structures previously identified through flow visualization by Tatterson and coworkers. Measurements are presented below in terms of

velocity vectors in both vertical (ϕ) planes, as well as in planes inclined at 45° to a ϕ plane, and therefore parallel to the inclination of the blades, in order to illustrate the trailing vortices and their origins at the blade tips.

Angle-resolved mean velocity vectors (the resultant vectors in vertical ϕ planes obtained from the measured axial and radial velocity components) are presented in Figure 4a–Figure 4g for seven ϕ angles, 0° (and therefore 90° also), 2°, 8°, 30°, 45°, 60° (which can also be considered as −30° before the blade) and 75° (−15°). Only the vectors measured in the region $0 < r/T < 0.20$ and $0.16 < z/T < 0.40$ are shown, as this is the region around the blade tip where trailing vortex activity is evident. In this figure the blades must be considered as moving out of the page toward the reader. The reader's attention is drawn to the fact that in Figure 4a–4g and especially Figure 4a–4c and 4f the blade cuts across the measurement plane and as a result some of the vectors show the flow in front and some behind the blade. In regions where the blade crosses the corresponding plane in each figure, either one or both velocity components could not be measured due to the blade presence. The edges of the blades are shown in all figures and a line has been drawn through the blade in those figures where the blade is crossing the plane of measurement (Figure 4a, 4b, 4c, and 4g) to indicate where the blade is intersected by the corresponding ϕ plane. This line is horizontal in Figure 4a ($\phi = 0°$) and inclined in Figures 4b, 4c, and 4g.

In the $\phi = 0°$ plane, Figure 4a, the flow around the blade under consideration (which is termed the leading blade hereafter) is directed mainly outward at the top (behind the blade), whereas that near the bottom (in front of the blade) is directed inward, toward the axis. The trailing vortex is the circulation centered around $r/T = 0.155$, $z/T = 0.34$; it is formed by the interaction of the streams issuing from the top and side of the blade and it is already developed and over 5 mm in diameter. The circulatory motion centered around $r/T = 0.16$ and $z/T = 0.24$ indicates the presence of the trailing vortex from the preceding blade, which is still in evidence 90° after that blade has crossed this plane.

The vectors in Figure 4b at $\phi = 2°$ give a good indication of the rapid development of the trailing vortex behind the leading blade: the vortex center is now found at a lower elevation. It is interesting to note that there is some evidence of circulation stemming from the vortex from the preceding

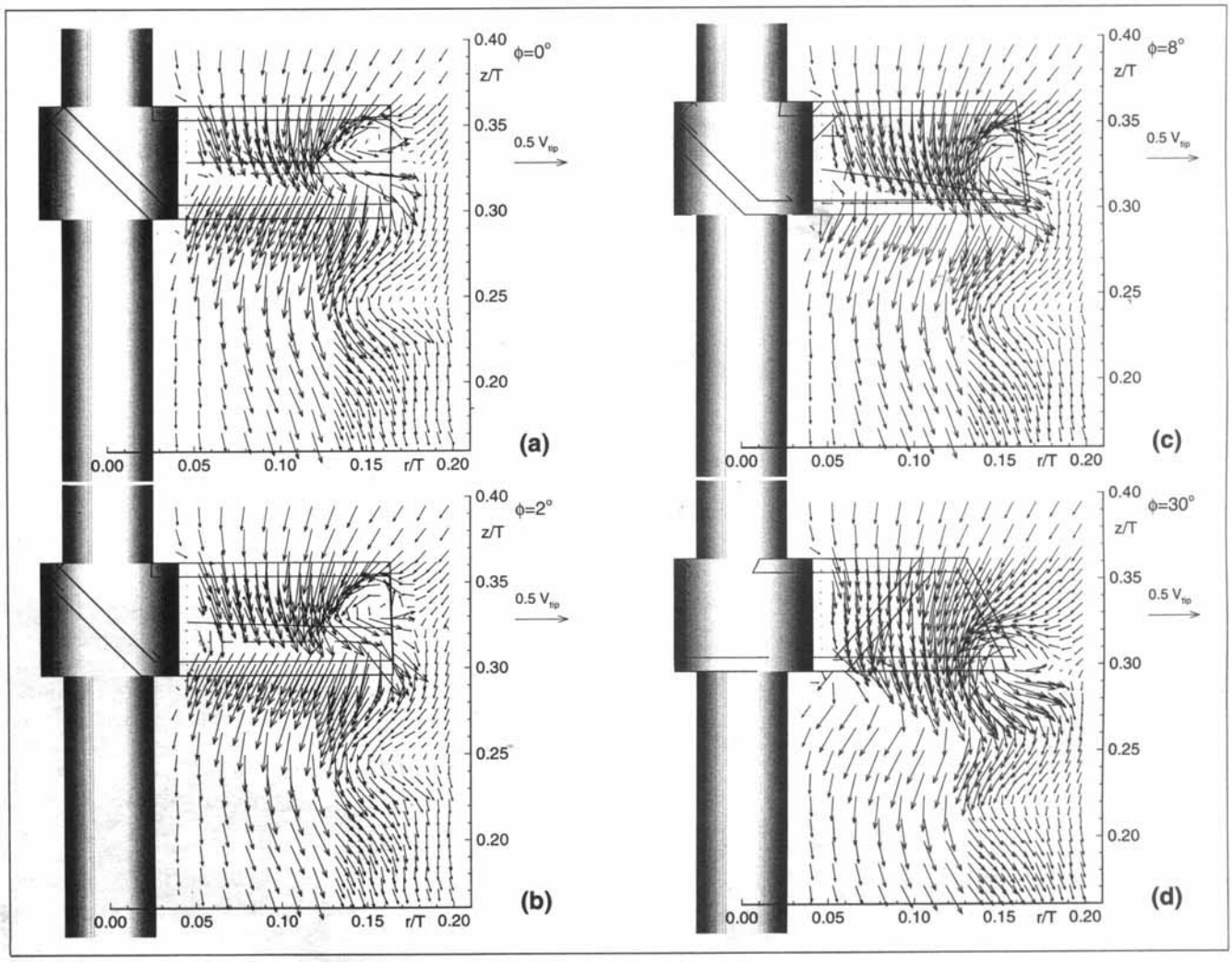

Figure 4. Angle-resolved mean velocity vectors in the vicinity of the impeller blade in seven ϕ planes: (a) $\phi = 0°$; (b) $\phi = 2°$; (c) $\phi = 8°$, (d) $\phi = 30°$. (Continued on next page.)

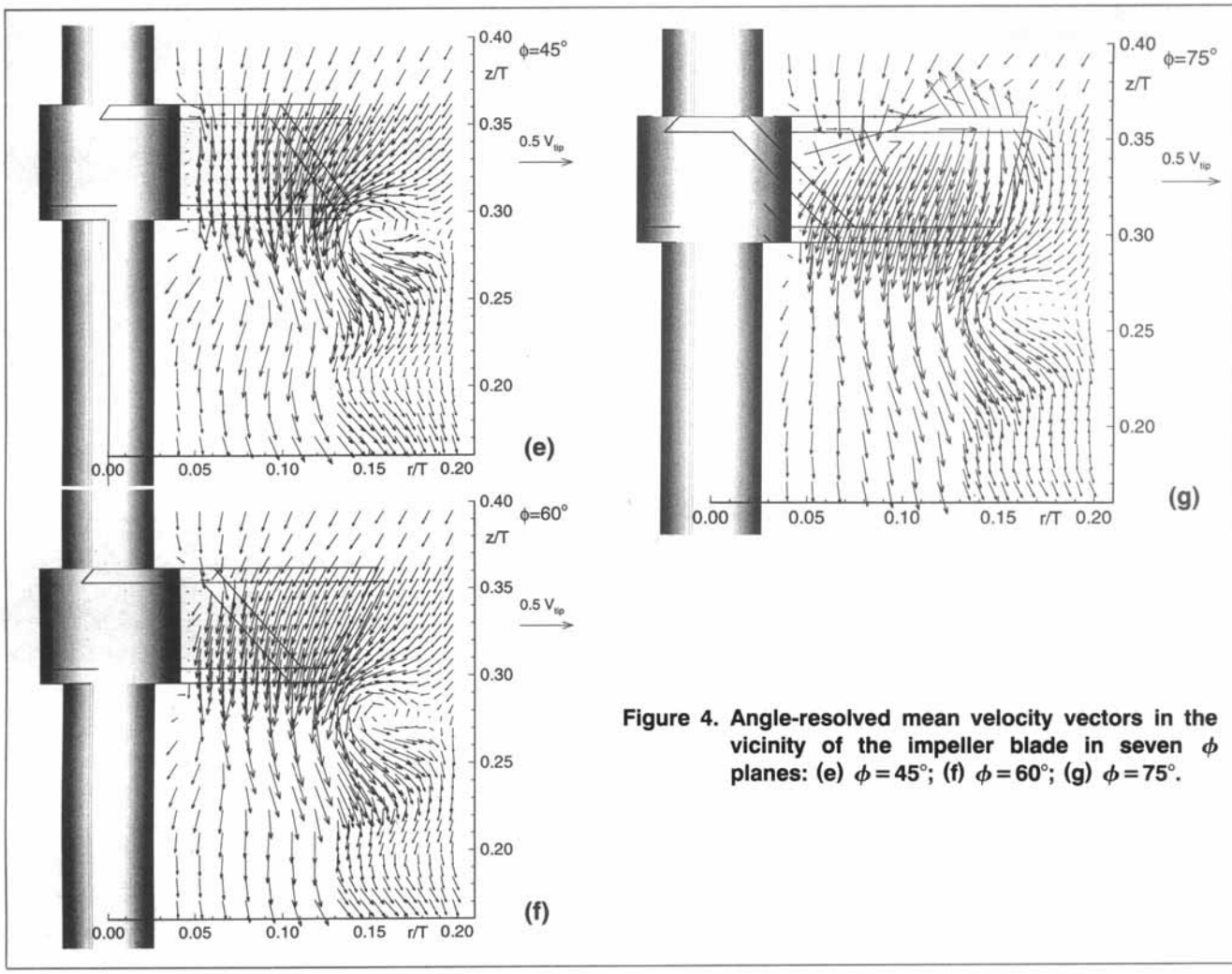

Figure 4. Angle-resolved mean velocity vectors in the vicinity of the impeller blade in seven ϕ planes: (e) $\phi = 45°$; (f) $\phi = 60°$; (g) $\phi = 75°$.

blade, which is centered around $r/T = 0.164$ and $z/T = 0.24$. The different directions of the flows over the front (lower part, inward) and back (upper part, outward) of the blade can also be seen in this plane, as in the following one, $\phi = 8°$ (Figure 4c).

The trailing vortex movement is best traced by the motion of its center, which moves down with increasing ϕ, following a path of nearly constant radius (similar to the blade radius). It is located at $r/T = 0.16$, $z/T = 0.30$ at $\phi = 30°$ (Figure 4d) and remains at essentially the same radius, following a helical path with increasing ϕ. The vortex axis is inclined at 20° to the horizontal: Figures 4e–4g illustrate this change of location with blade angle and is discussed further below. Therefore what is seen in the ϕ planes presented here is an inclined cross section of the vortex: however, as the radius of the center varies only a little with ϕ, and the inclination angle is small, Figure 4a–4g provide a good representation of the trailing vortex development.

It is interesting to follow the development of the trailing vortex from the preceding blade at $\phi = 30°$ (or 120° after the preceding blade) and 45° (or 135°). There is little evidence of the preceding blade vortex at the latter angle, and the results showed that each vortex persists for around 130°–140° behind the corresponding blade before it is merged with the turbulent bulk flow in the vessel. As can be seen in Figure 4g, the vectors at $\phi = 75°$ (or $-15°$ before the following blade) also indicate the flow over the top of the blade at $z/T = 0.36$ as the inclined blade approaches the measurement plane.

The cross section of the trailing vortex is oval and the vortex core increases in size with distance from the blade, as discussed below. The circumferential velocity at the vortex edge decreases approximately linearly with ϕ from around 0.55 V_{tip} at $\phi = 15°$ (not shown) to 0.35 V_{tip} at $\phi = 120°$. Ali et al. (1981) estimated the vortex circumferential velocities for the PBT to be around 0.25 V_{tip} for all rotational speeds studied, whereas they were nearly equal to V_{tip} for the Rushton impeller. The fact that the vortex circumferential velocity is a constant fraction of V_{tip} is in agreement with the work of van't Riet and Smith (1975) for Rushton turbine trailing vortices. It is worth noting, however, that the detailed Rushton trailing vortex measurements with LDA by Yianneskis et al. (1987) have showed that in planes perpendicular to the trailing vortex axis the circumferential velocities did not exceed 0.5 V_{tip} at around 10° behind the blade. The differences between both the present data and those of Yianneskis et al. and the flow visualization estimates of Ali et al. and van't Riet and Smith just given may stem partly from varying definitions of the vortex edge, and so on, but clearly the visual-

ization estimates can provide only approximate values. The convected axial velocity of the vortex may be estimated from the tip speed and the angle of the vortices with respect to the horizontal plane (V_{tip} sin 20° = 0.34 V_{tip}). This value is similar to that estimated by Ali et al. (0.3 V_{tip}) for Re = 115,000.

The resultant axial and radial mean velocity vectors in four planes inclined at 45°to the $\theta = 0°$ vertical plane are shown in Figure 5a–5d: the blade is located at ϕ angles of 80° (i.e., −10° before the blade), 0°, 4°, and 15°, respectively. Interpretation of the flow patterns shown and comparisons with the vectors in vertical (ϕ) planes should be made with care due to the strongly 3-D nature of the vortical flow around the blade, and as the vector locations, except for those at the central part of the region shown, do not coincide with those at the corresponding ϕ planes in Figure 4. The blade should be considered to move into the plane of the paper in these figures.

The flow in front of the blade (Figure 5a) is essentially akin to a boundary layer with no evidence of a recirculation. The flow is directed outward over the top part and inward over the lower part of the blade. Immediately behind the blade (Figure 5b), the vectors indicate the interaction of the fluid streams from the side and top edges of the blade, which in this plane start to produce the vortical motion, as indicated by the clockwise rotation evident from the vectors. It should be noted that, although the blade surface is actually located at $\phi = 0°$, it was possible to obtain results in this plane due to the finite size of the ϕ angle interval over which the measurements are made.

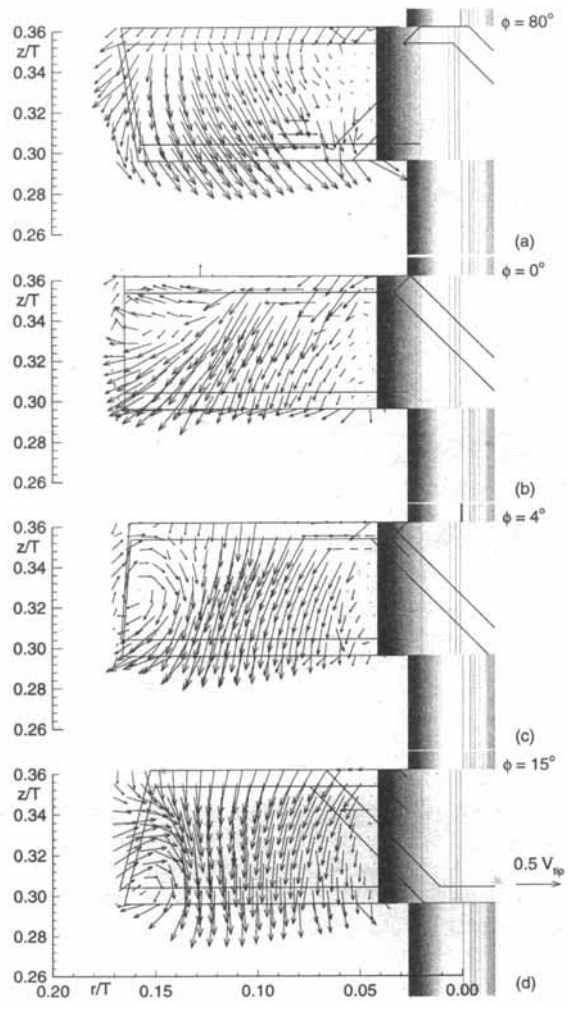

Figure 5. Angle-resolved mean velocity vectors near the blade in four planes inclined at 45° to the horizontal plane.

Each of these planes intersects the following ϕ plane at midblade: (a) $\phi = 80°$ (−10°); (b) $\phi = 0°$; (c) $\phi = 4°$; and (d) $\phi = 15°$.

The formation of the trailing vortex is more evident in Figure 5c, when the blade is at $\phi = 4°$. The flow is unidirectional over three-quarters of the blade-swept area, as in the previous two figures. The vortex center is located at midblade and a radius of around r/T = 0.151–0.158. With the blade at ϕ = 15° (Figure 5d), the vortical motion is centered close to the lower tip of the blade and at a similar radial distance. The change of the flow direction under the blade (inward, i.e., toward the axis at $\phi = 80°$, outward at $\phi = 0°$, and vertically downward at $\phi = 15°$) is noteworthy and similar to the observations of Hockey and Nouri (1996) for a 6-bladed 60° PBT.

The results in these 45° inclined planes indicate that the flow both immediately in front and behind the blade has magnitudes of around 0.5 V_{tip}. This is in agreement with the observation of Tatterson et al. (1980) that velocities in front and back of the blade are approximately the same, but their value of 0.25 V_{tip} was based on visualization observations and is probably an underestimation. In addition, there is no evidence of a second small and weak circulation at the upper tip of the blade, as inferred by Kresta and Wood (1993a) from their tuft flow visualization. The present data show clearly that the circulation near the upper blade tip is part of a single trailing vortex.

The trailing vortex is of spiral shape and is formed primarily by the interaction of the flow along the blade edge from the lower (upstream) surface in front of the blade that moves away from the vessel axis at the blade edge and that over the upper (downstream) surface behind the blade that moves toward the vessel axis (see, for example, Figure 5a and 5d, respectively). These flow motions produce the characteristic helical vortex pattern encountered at the tips of wings of finite span with positive lift (Duncan et al., 1970).

As mentioned earlier, the inclination of the helical axis to the horizontal is 20°. This angle is similar to those reported by Ali et al. (13°–18° at different Re's), but is should be noted that they measured the vertical angle between the horizontal and the top edge of the vortex, which will invariably be smaller than the angle formed by the axis, as the vortex diameter varies with distance from the blade. However, they quoted standard deviations of 22–25% in the values determined from their flow visualization tests and do not provide actual vortex sizes so that the axis inclination can be estimated. In addition, the variation of the angle of the axis to the horizontal (γ) with Re was estimated from the present results (Re = 7,300) and those of Ali et al. (Re = 115,000–240,000); it was found to be approximately linear (correlation coefficient of curve fit = 0.982) and is given in radians by

$$\gamma = 0.36 - 5.29 \times 10^{-7} Re. \qquad (3)$$

The normalized coordinates of the vortex axis ($z/T, r/T$) vary with ϕ in the manner shown in Figure 6a. The radial

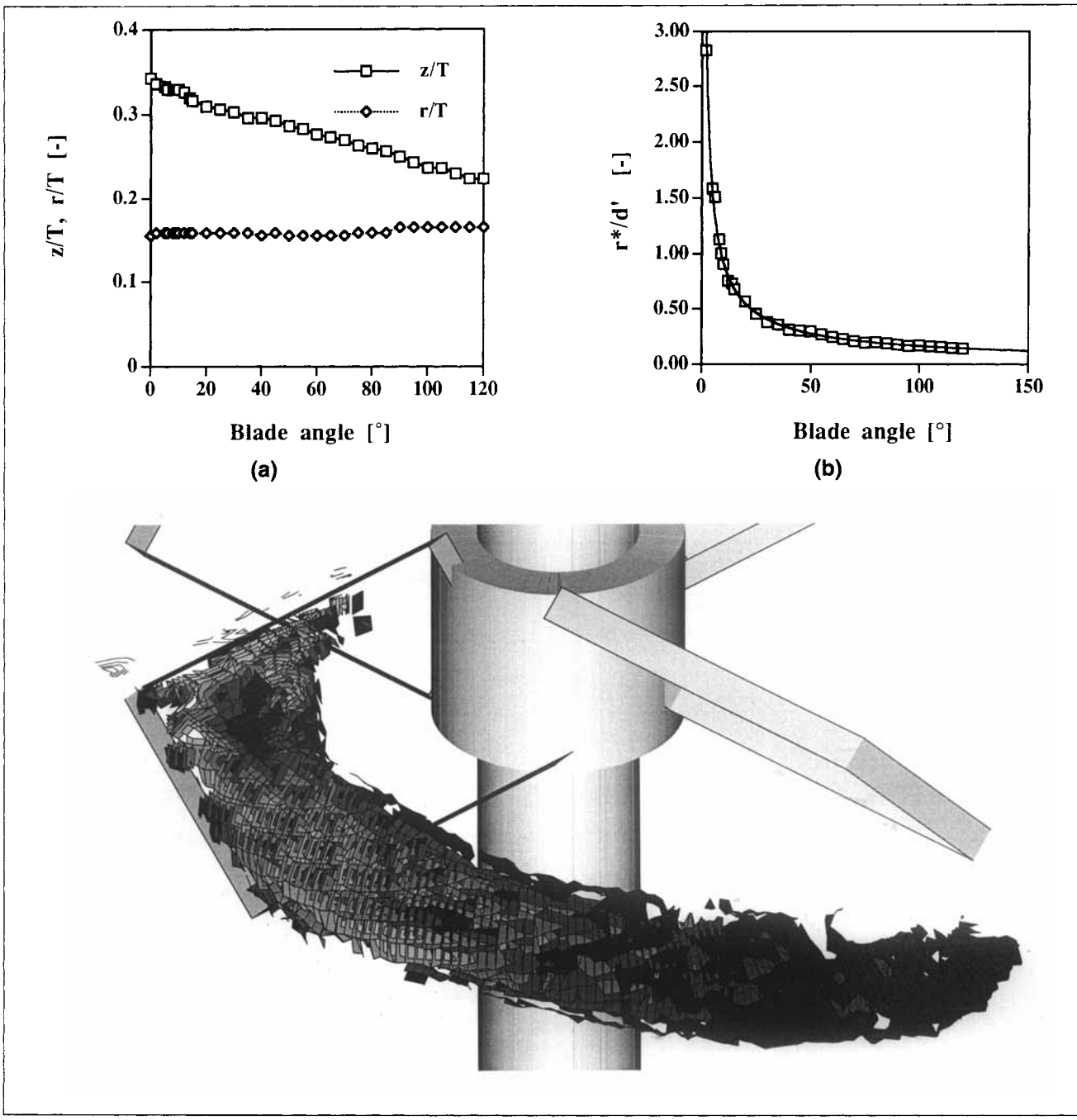

Figure 6. (a) Variation of the normalized coordinates r/T, z/T of the vortex axis with blade angle ϕ; (b) variation of the vortex radius normalized with distance from the blade along the vortex axis (r^*/d') with blade angle ϕ; (c) isosurface of vorticity at the edge of the trailing vortex behind an impeller blade.

distance of the center is practically constant: $r/T = 0.16$ (within ± 0.005 T) along the entire vortex path. The axis is found at lower axial locations with increasing ϕ: the variation of z/T with ϕ is approximately linear (correlation coefficient is 0.997) and can be described, again within ± 0.005 T, by

$$z/T = 0.335 - 0.054\phi, \tag{4}$$

where ϕ is in radians.

Albeit that the vortex axis is inclined to the horizontal, the vortex center location can be accurately determined from the velocity vectors in ϕ planes due to the density of the measurement grid and the relatively small inclination angle. It is more difficult, however, to determine the variation of the vortex core radius with ϕ from the velocity vectors, and attempts were made to find the core radius from contours of the vorticity (ζ) in ϕ planes, given by

$$\zeta = \frac{\partial V}{\partial z} - \frac{\partial U}{\partial r}. \tag{5}$$

The inclination of the vortex axis, the oval shape of the vortex, and the three-dimensionality of the flow make this task more onerous than determining the vortex axis, and the following observations therefore involve some approximations. The development of the vortex radius with ϕ, normalized by the distance from the blade *along the vortex axis*, d', is shown in Figure 6b. The trailing edge of the blade is located at $\phi = 12°$, where $d' = 5.3$ mm. The normalized radius can be approximated (correlation coefficient of curve fit = 0.999) by

$$r^*/d' = 0.25\phi^{-0.75}, \tag{6}$$

where ϕ is in radians. The maximum vortex diameter is approximately 0.3 D. Ali et al. observed that the diameter of the vortex was smallest behind the trailing edge of the blade and expanded linearly with distance from the trailing edge of the blade as more fluid entrained into the vortex. The vortex diameter was estimated as 0.25–0.33 of the distance from the blade tip for all speeds studied, and the shape and size of the vortices remained fairly consistent for all the observations. Figure 6b and Eq. 6 indicate that r^*/d' is around 0.50–0.66 (i.e., the vortex diameter is 0.25–0.33 of the distance from the blade) only for $15° < \phi < 30°$, whereas it is higher for lower ϕ and lower for higher ϕ values, respectively.

A representation of the extent of the trailing vortex is given by the vorticity contours shown in Figure 6c, for which locations where $\zeta = 330\ s^{-1}$ were defined as the edge of the vortex. It can be seen that the vortex extends to around 135° behind a blade, and vorticity originates at the side and upper tips of the blade.

RMS velocities and kinetic energy of turbulence

Contours of the turbulence kinetic energy obtained from data ensemble-averaged over 90° of revolution in the $\theta = 0°$ plane are shown in Figure 7. These contour values include the mean flow variation contribution due to the periodicity of the flow. The highest k/V_{tip}^2 levels, around 0.04–0.085 k/V_{tip}^2, are located in the region $0.20 < z/T < 0.36$ and $0.12 < r/T < 0.21$ and are associated with the presence of the trailing vortices. The k/V_{tip}^2 values in the bulk flow above and to the side of the impeller do not exceed in general 0.015, while below the blade, for $r/T < 0.2$, they are around 0.02–0.04.

These values may be compared with those of Kresta and Wood (1993b), but only approximately, as these authors used a $D = T/2$ PBT at a clearance of $C = T/4$. They reported a peak value of k/V_{tip}^2 of around 0.1 at the impeller discharge and values of around 0.023 in the region between the impeller stream and the axis of the vessel. The latter value is akin to those in similar regions in the present work, but the former is 18% higher than the peak k/V_{tip}^2 value of 0.085 mentioned earlier. This difference may stem partly from the difference in impeller clearance and diameter. In addition, Kresta and Wood's values are based on 360° ensemble-averages, and there may be some broadening due to blade-to-blade variations: such variations are expected to be very small in the present vessel, as the shaft was attached to a bearing in the vessel bottom and therefore shaft/impeller wobble (which may lead to blade-to-blade variations) was minimized.

Comparison of the k/V_{tip}^2 contours of Figure 7 with the corresponding ones in Figure 8, which are drawn from the

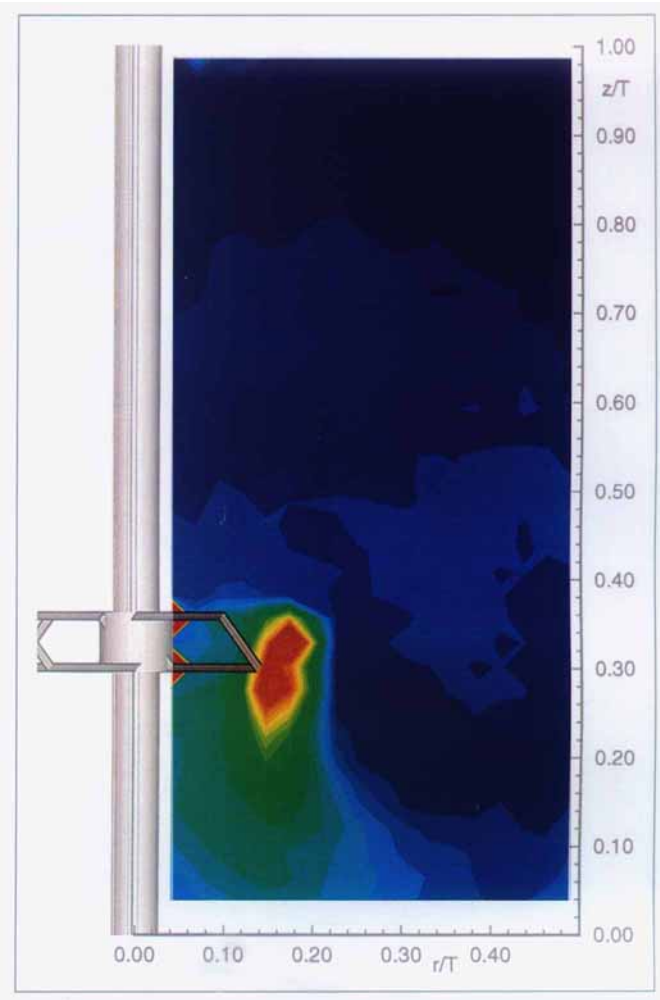

Figure 7. Contours of the normalized kinetic energy of turbulence (k/V_{tip}^2), ensemble-averaged over 90° of revolution, in the $\theta = 0°$ plane.

Contour values as for Figure 8.

angle-resolved values in the $\phi = 45°$ plane, that is, obtained as ensemble-averages over 1° of revolution, indicates clearly the broadening of the k levels due to the periodic contribution. The highest k/V_{tip}^2 values in Figure 8 are found in the region where the trailing vortex was identified in the vector plots presented earlier (Figure 4e), and they are around 0.058. The overestimation of the maximum k/V_{tip}^2 values in the 90° ensemble-averages of Figure 7 is therefore around 50%. In addition, the region of high k/V_{tip}^2 is considerably smaller than that shown by the 90° averaged values, approximately 8 mm in diameter and similar to the area where a distinct circulation could be observed in the vector plot of Figure 4e. Hockey and Nouri (1996) also observed that the ensemble-averaged rms values were up to two times higher than the corresponding angle-resolved values, due to the contribution of the mean flow variation included in the former, and that these differences became negligible at distances of two blade heights below the impeller and radii greater than 0.55 of the impeller radius. Conversely, in some locations near the blades and in some blade angles the ensemble-averaged values underestimate the levels of turbulence, for example, at $r/T =$

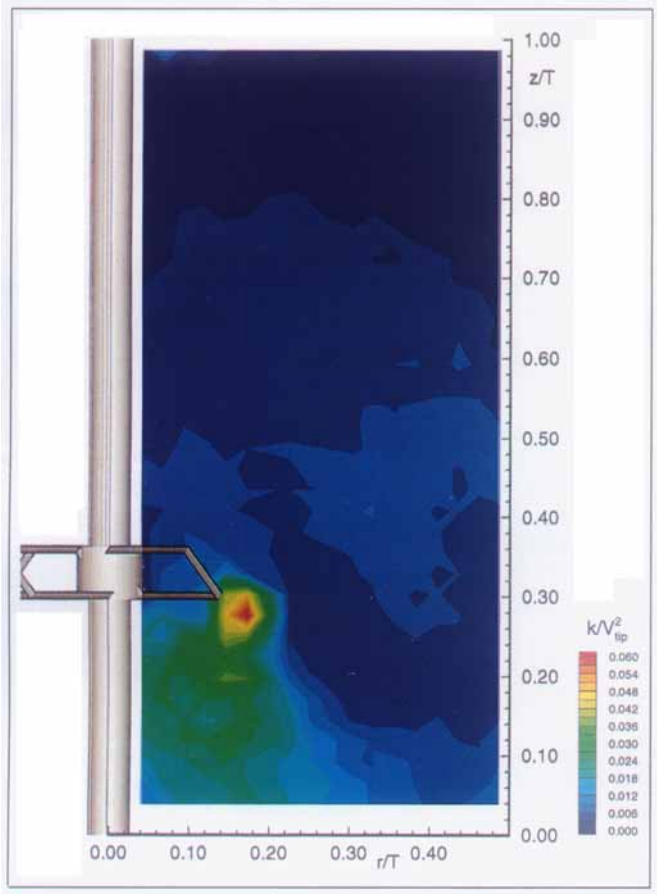

Figure 8. Contours of the angle-resolved normalized kinetic energy of turbulence (k/V_{tip}^2) in the $\phi = 45°$ plane.

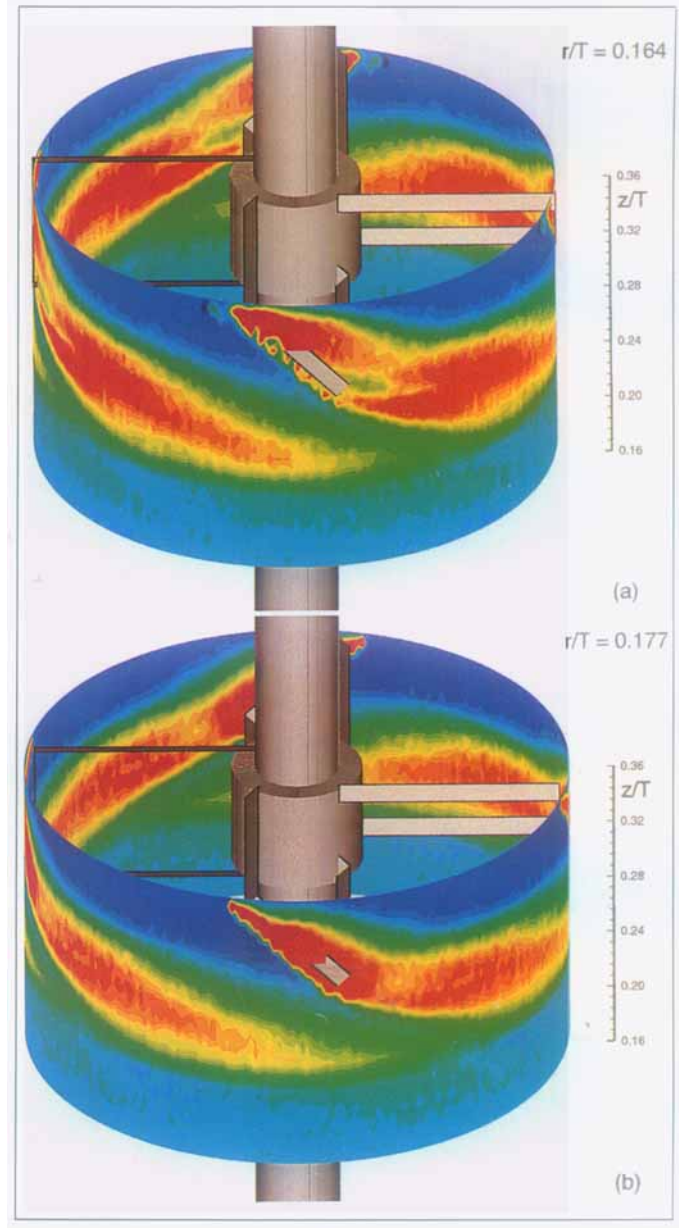

Figure 9. Contours of the angle-resolved normalized kinetic energy of turbulence (k/V_{tip}^2): (a) in the $r/T = 0.164$ plane; and (b) in the $r/T = 0.177$ plane.

Contour values as for Figure 8.

0.15 and $z/T = 0.20$ (compare Figures 7 and 8). This underestimation is of similar magnitude to the overestimation mentioned before and is also important for the proper characterization of turbulence in the vessel.

Contours of angle-resolved k/V_{tip}^2 are shown in various planes below, as they give a very good indication of the extent of vortical and turbulent activity in stirred vessels (see, e.g., Rutherford et al., 1996a) and give important information as to where in the vessel mixing is likely to be achieved faster and therefore where insertion of reactants, and so forth, should be made.

The contours of k/V_{tip}^2 in two cylindrical planes at $r/T = 0.164$ and 0.177 are shown in Figures 9a and 9b, respectively. The high k/V_{tip}^2 contours (0.03–0.06) indicate clearly the high turbulence associated with the evolution of the trailing vortex behind the blade. Regions with the highest values of k/V_{tip}^2 at $r/T = 0.164$ are observed to trail the upper and lower tips of the blade as shown in Figure 9a). Upstream of the blade the k values are over 10 times lower than inside the vortex, while 1.5 blade widths below the lower tip they are 3 times lower. The contours at $r/T = 0.177$ (Figure 9b) indicate that the vortex dissipates rapidly with radial distance and the high k/V_{tip}^2 core has descreased significantly over a radial distance of only 0.02 T.

Projection of the k/V_{tip}^2 contours in this cylindrical plane onto a flat surface (not shown for brevity) enabled the confirmation of the inclination of the vortex axis (20°), and the vortex, as evidence by high k/V_{tip}^2 values, persisted for 135°, that is, up to 45° behind the following blade. Another good indication of the extent of the vortices is given by the k/V_{tip}^2 contours in the $z/T = 0.29$ horizontal plane shown in Figure 10. These contours show high k/V_{tip}^2 values at the lower tip of the blade, which extend to the following blade and over a horizontal area that is, at its maximum, 0.135 T wide.

A good indication of the generation and decay of turbulence in the vortices can be provided by comparing the maximum k/V_{tip}^2 value inside the vortex with the corresponding value at its edge. The development of these values with blade

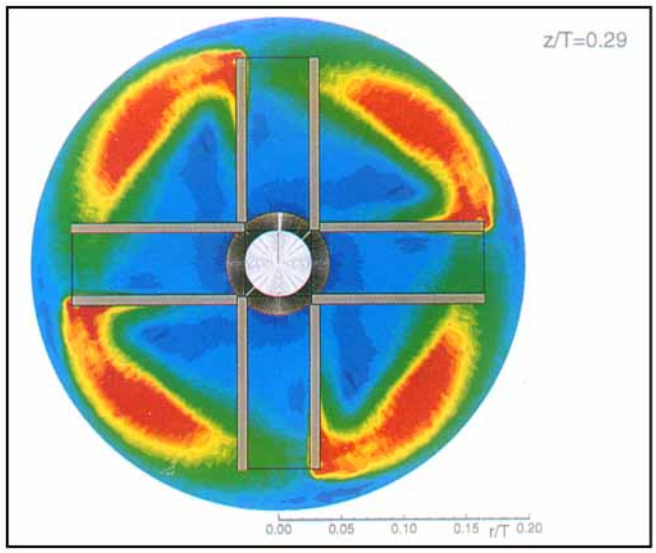

Figure 10. Contours of the angle-resolved normalized kinetic energy of turbulence (k/V_{tip}^2) in the $z/T = 0.29$ plane (contour values as for Figure 8).

angle ϕ along the vortex path is shown in Figure 11. It can be clearly seen that the maximum k/V_{tip}^2 increases with ϕ (to 0.077) at 60° and subsequently decreases until 150°, while the k/V_{tip}^2 values at the vortex edge are considerably lower and increase from 0.01 near the blade to 0.03 at 150°, where they are nearly identical with the maximum k/V_{tip}^2 values. After 150°, both values decrease sharply. This finding is important, as it indicates that the intense turbulence energy generated in the vortices is contained within a relatively small region and dissipates rapidly; this energy could be harnessed to aid mixing but the location(s) of the insertion of reactants, feed pipes, and so forth, must be selected with care to ensure utilization of these high levels of turbulence.

Isotropy of the turbulence

In order to ascertain whether the turbulence, especially in the impeller discharge, is isotropic, the distributions of the three turbulence levels throughout the measurement region

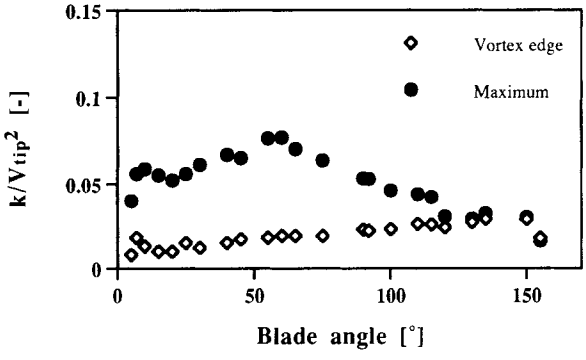

Figure 11. Variation of the maximum and vortex-edge values of k/V_{tip}^2 with blade angle ϕ.

were compared. Anisotropic turbulence was previously measured in the impeller streams issuing from Rushton impellers (Rutherford et al. 1996a), and it is well known that CFD predictions of the flows in stirred vessels may underestimate considerably the levels of k in the impeller stream, while CFD methods with turbulence models, which include anisotropic eddy viscosity formulations, perform better (Lee et al., 1996; Rutherford et al., 1996a,b).

The turbulence levels of the axial and tangential components were compared with the radial component to quantify the degree of isotropy/anisotropy of the turbulence in the vicinity of the impeller. It should be noted, however, that although both the u'/v' and w'/v' values may vary considerably in the impeller stream, there are large values of u'/v' and especially w'/v' in locations where the turbulence levels are somewhat similar. This is due to the relative magnitudes of the turbulence levels: for example, for $w' = 0.02$ m/s and $v' = 0.01$ m/s, $w'/v' = 2.0$, whereas in absolute terms the levels are similar and within experimental error. A better way to assess the degree of isotropy is by considering the absolute difference between the different turbulence levels normalized by V_{tip}, that is, $|u' - v'|/V_{tip}$ and $|w' - v'|/V_{tip}$. When these values tend to zero, $u' \to v'$ and $w' \to v'$ and the turbulence may be considered isotropic.

Contours of $|u' - v'|/V_{tip}$ in the $\phi = 45°$ plane are shown in Figure 12. Regions of locally high values (0.1–0.15) of $|u' - v'|/V_{tip}$ can be observed below and near the impeller blade. Most other flow regions have values of $|u' - v'|/V_{tip}$ between 0.00 and 0.06. In these regions, the turbulence can be considered to be isotropic. Similarly, locally high values of $|w' - v'|/V_{tip}$ were also found near the blade.

Hockey and Nouri (1996) also measured anisotropic turbulence levels in the impeller stream. Kresta and Wood (1993b) found that in the impeller discharge of their vessel the three rms velocity components differed by 25–50% and concluded that local isotropy may be assumed. The present findings as well as those of Hockey and Nouri indicate that the approximation of isotropic turbulence in the impeller stream may not be appropriate and CFD modeling of the flows might have to take this into account.

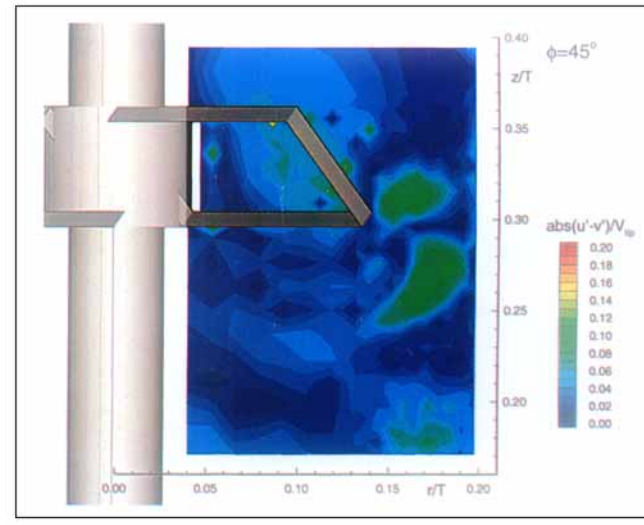

Figure 12. Contours of $|u' - v'|/V_{tip}$ in the $\phi = 45°$ plane.

Concluding Remarks

LDA results obtained in a 152-mm-diameter vessel have been presented, and the flow field and turbulence structure produced by a 4-bladed 45° PBT have been described in detail. The LDA data presented provide the only quantitative results available on the extent, magnitude, velocity, and turbulence distribution of the trailing vortices produced by pitched-blade impellers.

The flow in the vessel includes essentially a main circulation ring vortex of low turbulence, a smaller ring vortex circulation on the bottom near the axis, and a trailing vortex formed around each blade. The size, shape, and location of the vortices are compared with the results of earlier flow visualization studies. A single trailing vortex is formed behind each blade from the interaction of the fluid streams issuing from the side, upper, and lower edges of the blade. The circumferential velocity in the vortex decays almost linearly with distance from the blade. The velocities in the vortex are around 0.5 V_{tip} near the blade. The vortex diameter increases with the distance from the blade. Near the blade, the vortex occupies almost a fifth of the blade radial width. The vortex axis is inclined at 20° to the horizontal and its radius (as identified from iso-vorticity contours) is essentially constant over the 130°–140° over which the vortex can be distinguished.

The levels of turbulence energy outside the vortices are around an order of magnitude lower than inside: the vortices provide the primary source of turbulence generation in the vessel, but are dissipated into the bulk flow 135° behind and 1.5 blade widths below each blade. Knowledge of the vortex location and size could prove to be most beneficial for efficient blending of fluids with such impellers: mixing times could be significantly reduced if the trailing vortices are used for the location of feed streams, and so on. The concentrated high turbulence levels generated close to the impeller in the vortices could therefore be exploited for the optimization of blending operations, and knowledge of the effect of the vortices on the concentration field is urgently required, which should, together with the present work, prove useful for mixing process design.

The measurements presented herein provide the most comprehensive data set of the mean flow and turbulence field in a vessel stirred by an axial-flow impeller reported to date and should also prove very useful for the validation of future CFD predictions of the flow.

Acknowledgment

The authors acknowledge financial support provided by the Commission of the European Union under the BRITE EURAM Programme, Contract BRPR-CT96-0185.

Notation

D = impeller diameter, m
r = radial coordinate: distance from the axis of the vessel, m
r^* = trailing vortex radius, m
T = vessel diameter, m
V_{tip} = impeller tip speed ($= \pi ND/60$), m/s
z = axial coordinate of the measurement volume, m
ν = kinematic viscosity of fluid, m^2/s

Literature Cited

Ali, A. M., H. H. S. Yuan, D. S. Dickey, and G. B. Tatterson, "Liquid Dispersion Mechanisms in Agitated Tanks: Part I. Pitched Blade Turbine," *Chem. Eng. Commun.*, **10**, 205 (1981).

Armstrong, S. G., and S. Ruszkowski, "Measurement and Comparison of Flows Generated by Different Types of Impeller in a Stirred Tank," *Proc. Colloq. on Mechanical Agitation*, France, E.N.S.I.G.C., Toulouse, p. 1.9 (1987).

Distelhoff, M. F. W., J. Laker, A. J. Marquis, and J. M. Nouri, "The Application of a Strain Gauge Technique to Measurement of the Power Dissipation of Five Impellers," *Exp. Fluids*, **20**, 56 (1995).

Duncan, W. J., A. S. Thom, and A. D. Young, *Mechanics of Fluids*, Arnold, London (1970).

Hockey, R. M., *Turbulence Newtonian and Non-Newtonian Flows in a Stirred Reactor*, PhD Thesis, Univ. of London, London (1990).

Hockey, R. M., and J. M. Nouri, "Turbulent Flow in a Baffled Vessel Stirred by a 60° Pitched Blade Impeller," *Chem. Eng. Sci.*, **51** (19), 4405 (1996).

Höfken, M., M. Schäfer, and F. Durst, "Detaillierte Untersuchung des Strömungsefeldes innerhalb eines Sechs-Blatt-Scheibenrührers," *Chem. Ing. Tech.*, **68**, 803 (1996).

Jaworski, Z., A. W. Nienow, E. Koutsakos, K. Dyster, and W. Bujalski, "An LDA Study of Turbulent Flow in a Baffled Vessel Agitated by a Pitched Blade Turbine," *Trans. Inst. Chem. Eng.*, **69**, Part A, 313 (1991).

Kresta, S. M., and P. E. Wood, "The Mean Flow Field Produced by a 45° Pitched Blade Turbine: Changes in the Circulation Pattern Due to Off Bottom Clearance," *Can. J. Chem. Eng.*, **71**, 42 (1993a).

Kresta, S. M., and P. E. Wood, "The Flow Field Produced by a Pitched Blade Turbine: Characterisation of the Turbulence and Estimation of the Dissipation Rate," *Chem. Eng. Sci.*, **48**, 1761 (1993b).

Lee, K. C., K. Ng, M. Yianneskis, F. Lange, and R. Sanatian, "Sliding Mesh Predictions of the Flows Around Rushton Impellers," *Inst. Chem. Eng. Symp. Ser.*, **140**, 47 (1996).

Nouri, J. M., and J. H. Whitelaw, "Flow Characteristics of Stirred Reactors with Newtonian and Non-Newtonian Fluids," *AIChE J.*, **36**, 627 (1990a).

Nouri, J. M., and J. H. Whitelaw, "Effect of Size and Confinement on the Flow Characteristics in Stirred Reactors," *Proc. Int. Symp. on Application of Laser Techniques to Fluid Mechanics*, Lisbon, Portugal, p. 23.2.1 (1990b).

Ranade, V. V., and J. B. Joshi, "Flow Generated by Pitched Blade Turbines I: Measurements Using Laser Doppler Anemometer," *Chem. Eng. Commun.*, **81**, 197 (1989).

Rao, K. S., V. B. Rewatkar, and J. B. Joshi, "Critical Impeller Speed for Solid Suspension in Mechanically Agitated Contactors," *AIChE J.*, **34**, 1332 (1988).

Rutherford, K., K. C. Lee, S. M. S. Mahmoudi, and M. Yianneskis, "Hydrodynamic Characteristics of Dual Rushton Impeller Stirred Vessels," *AIChE J.*, **42**(2), 332 (1996a).

Rutherford, K., K. C. Lee, S. M. S. Mahmoudi, and M. Yianneskis, "The Influence of Rushton Impeller Blade and Disk Thickness on the Mixing Characteristics of Stirred Vessels," *Trans. Inst. Chem. Eng.*, Part A, **74**, 369 (1996b).

Schäfer, M., M. Höfken, and F. Durst, "Detailed LDV Measurements for Visualization of the Flow Field Within a Stirred Tank Reactor Equipped with a Rushton Turbine," *Trans. Inst. Chem. Eng.*, Part A, **75**, 279 (1997).

Sheu, Y.-H. E., T. P. K. Chang, G. B. Tatterson, and D. S. Dickey, "A Three-Dimensional Measurement Technique for Turbulent Flows," *Chem. Eng. Commun.*, **17**, 67 (1982).

Stoots, C. M., and R. V. Calabrese, "The Mean Velocity Field Relative to a Rushton Turbine Blade," *AIChE J.*, **41**(1), 1 (1995).

Tatterson, G. B., and T. G. Stanford, "Liquid Dispersion Mechanisms in Agitated Tanks: III. Low Viscosity Discrete Phase into High Viscosity Continuous Phase," *Chem. Eng. Commun.*, **6**, 371 (1981).

Tatterson, G. B., H.-H. S. Yuan, and R. S. Brodkey, "Stereoscopic Visualization of the Flows for Pitched Blade Turbines," *Chem. Eng. Sci.*, **35**, 1369 (1980).

Tay, M., and G. B. Tatterson, "Form and Skin Drag Contributions to Power Consumption for the Pitched-Blade Turbine," *AIChE J.*, **31**(11), 1915 (1985).

Van't Riet, K., and J. M. Smith, "The Trailing Vortex System Produced by Rushton Turbine Agitators," *Chem. Eng. Sci.*, **30**, 1093 (1975).
Van't Riet, K., W. Bruijn, and J. M. Smith, "Real and Pseudo-Turbulence in the Discharge Stream from a Rushton Turbine," *Chem. Eng. Sci.*, **31**, 407 (1976).
Wu, H., and G. K. Patterson, "Laser-Doppler Measurements of Turbulent-Flow Parameters in a Stirred Mixer," *Chem. Eng. Sci.*, **44**(10), 2207 (1989).
Yianneskis, M., and J. H. Whitelaw, "On the Structure of the Trailing Vortices Around Rushton Turbine Blades," *Trans. Inst. Chem. Eng.*, Part A, **17**, 543 (1993).
Yianneskis, M., Z. Popiolek, and J. H. Whitelaw, "An Experimental Study of the Steady and Unsteady Flow Characteristics of Stirred Reactors," *J. Fluid Mech.*, **175**, 537 (1987).
Zwietering, T. N., "Suspending of Solid Particles in Liquid by Agitators," *Chem. Eng. Sci.*, **8**, 244 (1958).

Manuscript received Oct. 6, 1997, and revision received Feb. 18, 1998.